

Illinois State University

ISU ReD: Research and eData

---

Faculty Publications – Biological Sciences

Biological Sciences

---

2024

## KIF3A Tail Domain Phosphorylation Is Not Required for Ciliogenesis in Mouse Embryonic Fibroblasts

Ayoola Fasawe

*Illinois State University*, [ayoola.fasawe@gmail.com](mailto:ayoola.fasawe@gmail.com)

Jessica M. Adams

*Illinois State University*

Martin Engelke

*Illinois State University*, [mfengel@ilstu.edu](mailto:mfengel@ilstu.edu)

Follow this and additional works at: <https://ir.library.illinoisstate.edu/fpbiosci>



Part of the [Biology Commons](#), and the [Cell Biology Commons](#)

---

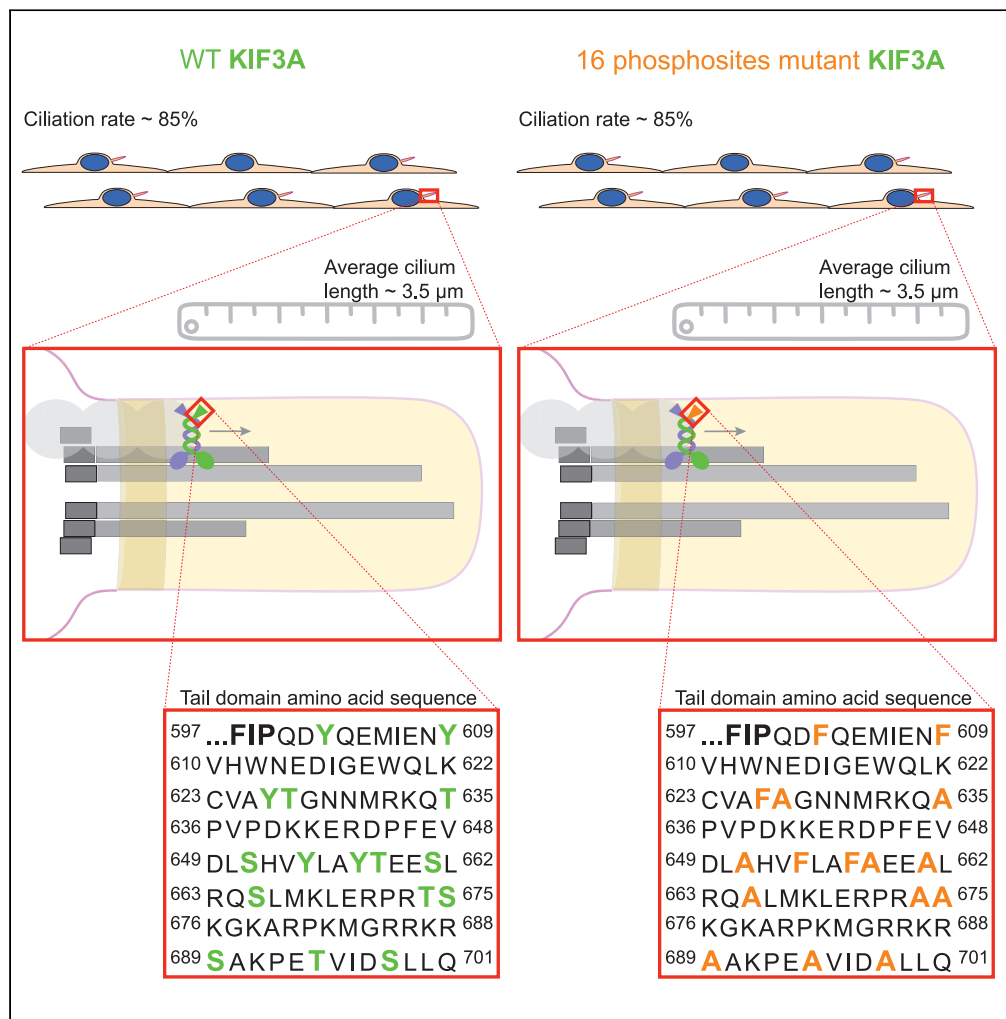
### Recommended Citation

Ayoola S. Fasawe, Jessica M. Adams, & Martin F. Engelke, "KIF3A tail domain phosphorylation is not required for ciliogenesis in mouse embryonic fibroblasts," *iScience*, 27, Issue 3, (2024): 109149.  
<https://doi.org/10.1016/j.isci.2024.109149>.

This Article is brought to you for free and open access by the Biological Sciences at ISU ReD: Research and eData. It has been accepted for inclusion in Faculty Publications – Biological Sciences by an authorized administrator of ISU ReD: Research and eData. For more information, please contact [ISUREd@ilstu.edu](mailto:ISUREd@ilstu.edu).

Article

# KIF3A tail domain phosphorylation is not required for ciliogenesis in mouse embryonic fibroblasts



Ayoola S. Fasawe,  
Jessica M. Adams,  
Martin F. Engelke

mfengel@ilstu.edu

**Highlights**

Mammalian KIF3A tail domain phosphorylation is not required for ciliogenesis

Mechanism regulating KIF3A/KIF3B/KAP3 for ciliogenesis remains elusive

Phenotypically silent modifications of KIF3A and KIF3B can have synthetic effects



## Article

## KIF3A tail domain phosphorylation is not required for ciliogenesis in mouse embryonic fibroblasts

Ayoola S. Fasawe,<sup>1</sup> Jessica M. Adams,<sup>1</sup> and Martin F. Engelke<sup>1,2,\*</sup>

## SUMMARY

Primary cilia are essential signaling organelles that protrude from most cells in the body. Heterodimeric kinesin-2 (KIF3A/KIF3B/KAP3) powers several intracellular transport processes, including intraflagellar transport (IFT), essential for ciliogenesis. A long-standing question is how a motor protein is differentially regulated for specific cargos. Since phosphorylation of the KIF3A tail domain was suggested to regulate the activity of kinesin-2 for ciliogenesis, similarly as for the cytosolic cargo N-Cadherin, we set out to map the phosphosites involved in this regulation. Using well-characterized *Kif3a*<sup>-/-</sup>; *Kif3b*<sup>-/-</sup> mouse embryonic fibroblasts, we performed ciliogenesis rescue assays with a library of phosphomimetic mutants comprising all predicted phosphosites in the KIF3A tail domain. In contrast to previous reports, we found that KIF3A tail domain phosphorylation is dispensable for ciliogenesis in mammals. Thus, mammalian kinesin-2 is differently regulated for IFT than currently thought, consistent with the idea of differential regulation for ciliary and cytosolic cargo.

## INTRODUCTION

Cilia are elongated organelles on the surface of most cells in the human body. These organelles are supported by a microtubule-based cytoskeleton called the axoneme. Motile cilia, or flagella, are necessary to power fluid flow over epithelia and generate cell motility. Primary cilia are essential to detect a wide variety of external stimuli, including morphogens, mechano-sensation, and light, in a tissue-specific manner. Given these critical functions, it is not surprising that ciliary malfunction gives rise to a plethora of human diseases called ciliopathies.<sup>1</sup>

One process that is required for the genesis, function, and structural maintenance of primary and motile cilia is intraflagellar transport (IFT): Motor proteins continuously transport IFT trains laden with ciliary cargo along axonemal microtubules. In mammals, heterodimeric kinesin-2, comprising two motor subunits (KIF3A/KIF3B) and a kinesin-associated protein (KAP3), imports IFT trains at the ciliary base and transports them to the axonemal tip. There, kinesin-2 disengages and the IFT trains are unloaded, reloaded, and rearranged for retrograde transport. Subsequently, cytoplasmic dynein-2 binds to the rearranged IFT trains to transport them back to the ciliary base for cargo export and IFT particle recycling.<sup>2-4</sup>

A current research question in the field is whether heterodimeric kinesin-2 is regulated for IFT by post-translational modifications.<sup>5</sup> Potential mechanisms for this motor regulation include a) switching the motor from the autoinhibited to the activated form and b) regulating cargo binding to the motor. Mutations in several kinases are linked to ciliopathies, making phosphorylation a prime candidate for IFT regulation.<sup>6</sup> Furthermore, several kinases and phosphatases have been implicated in cilium length regulation.<sup>7,8</sup> Indeed, phosphorylation of the tail domain of the KIF3B homolog Fla8 was reported to trigger cargo release at the ciliary tip in the single-celled, biflagellate algae *Chlamydomonas*.<sup>9</sup> Similar phosphorylation of KIF3B in mammals, where heterodimeric kinesin-2 is also essential for ciliogenesis, was deemed unlikely.<sup>10</sup> Instead, Chaya et al. identified the KIF3A tail as a phosphorylation target for Ciliogenesis-Associated Kinase 1 (CILK1; formerly ICK). In the same study, they reported that a KIF3A construct with eight serine and threonine residues in the tail mutated to the dephosphorylation mimetic alanines (KIF3A-8xA) was unable to rescue ciliogenesis in mouse embryonic fibroblasts in which *Kif3a* has been depleted via RNAi.<sup>11</sup> This suggested that in mammals, heterodimeric kinesin-2 might be regulated via phosphorylation of the KIF3A rather than the KIF3B tail domain.

In this study, we set out to test this hypothesis and to tease apart which of the eight serine and threonine residues mutated in KIF3A-8xA by Chaya et al. is critical for regulating heterodimeric kinesin-2 for ciliogenesis. We thus created a library of KIF3A expression constructs in which we replaced all potential phosphorylation sites in the KIF3A tail domain with phosphomimetic amino acids. We screened the constructs of the library for their ability to rescue ciliogenesis in *Kif3a*<sup>-/-</sup>; *Kif3b*<sup>-/-</sup> mouse embryonic fibroblasts (3T3 cells) and surprisingly found no evidence

<sup>1</sup>School of Biological Sciences, Cell Physiology, Illinois State University, Normal, IL 61790, USA

<sup>2</sup>Lead contact

\*Correspondence: mfengel@ilstu.edu

<https://doi.org/10.1016/j.isci.2024.109149>



for the requirement of KIF3A tail domain phosphorylation for regulating kinesin-2 for IFT and ciliogenesis. Thus, future studies will be needed to delineate how this motor is controlled for IFT.

## RESULTS

### Phosphorylation of previously reported serine and threonine residues in the KIF3A tail domain is not required for ciliogenesis

Originally, we set out to test phosphorylation of which of the eight serine (S) and threonine (T) residues in the C-terminal portion of the tail domain of KIF3A reported by Chaya et al. regulates kinesin-2 for ciliogenesis.<sup>11</sup> We thus generated a library of plasmids expressing KIF3A with individual (S) and (T) mutated to dephosphorylation (alanine, A) and phosphorylation (aspartate, D) mimetic residues (Figure 1A and Table 1). We then co-expressed each of the phosphosite mutant expressing plasmids with mNeonGreen (mNG)-tagged KIF3B in a line of well-characterized *Kif3a*<sup>-/-</sup>; *Kif3b*<sup>-/-</sup> double knockout 3T3 cells<sup>12</sup> and stimulated ciliogenesis via serum starvation. Since heterodimeric kinesin-2 is required for ciliogenesis in mammals, the double knockout cells cannot generate cilia unless transfected with plasmids expressing functional KIF3A and KIF3B. As expected, we found that cells transfected with an mNG-expressing control plasmid lacked cilia, whereas cells transfected with wildtype KIF3A and KIF3B-mNG generated cilia (Figure 1B). To our surprise, expression of all single dephosphorylation mimetic KIF3A mutants (S/T to A) rescued ciliogenesis and cilium length at levels comparable to wildtype KIF3A/KIF3B (Figures 1C, 1D, and S1). This raised the possibility that the simultaneous phosphorylation status of multiple phosphosites in the tail domain of KIF3A is relevant for ciliation. We thus generated a KIF3A expression plasmid in which, similar to Chaya et al., all eight phosphosites were mutated to A (8xA, Figure 2A). However, expression of 8xA did not reproduce the reported reduction in ciliogenesis rate and instead resulted in a ciliation rate and average cilium length that was not statistically significantly different from the wildtype motor (Figures 2C and 2D). One difference between the KIF3A-8xA construct used by Chaya et al. and our 8xA construct is the visualization tag. While we fused a myc-tag N-terminally to KIF3A, they used a FLAG tag. To determine if the disparate results were caused by the FLAG tag and because we were unable to determine if Chaya et al. used an N- or C-terminal fusion of the tag, we created both versions. However, expression of neither construct resulted in ciliation rates or average cilium lengths different from cells expressing wildtype KIF3A (Figures 3A and 3B'-3D'). Thus, the discrepancy must stem from other experimental differences as outlined in the discussion section.

The phosphorylation mimetic and the dephosphorylation mimetic status of important phosphosites in the tail domain of a motor can display different phenotypes. In *C. reinhardtii*, mutating the site S663 to a dephosphorylation mimetic (A) modestly reduced, whereas mutation to a phosphomimetic (D) completely abolished ciliogenesis.<sup>9</sup> We thus also generated and expressed eight KIF3A mutants in which the same eight phosphosites had been mutated one by one to the phosphomimetic amino acid (D). Except for the S698D mutant, which had a slightly but significantly reduced ciliation rate, all other conditions resulted in ciliation rates and average cilium length indistinguishable from cells expressing wildtype KIF3A (Figures 1E, 1F, and S1). Furthermore, grouping the phosphomimetic mutations of all eight phosphosites (8xD) closely phenocopied the S698D mutation (Figures 2B-2D). These results indicate that the phosphorylation status of eight selected (S) and (T) residues in the C-terminal portion of the KIF3A tail domain is largely dispensable for regulating heterodimeric kinesin-2 for ciliogenesis.

### Mutation of additional potential phosphosites in the KIF3A tail domain impairs ciliogenesis

We next examined the KIF3A tail domain for further potential phosphosites that affect the motor's ability to drive ciliogenesis. We identified eight additional residues and grouped them into two groups according to their NetPhos-3.1 (DTU Health Tech, Denmark) prediction scores (Figures 2A and Table 1). One group encompassing high prediction scores (>0.500) contained two tyrosine (Y) and one (T). The group with low prediction scores (0.391-0.455) included all three residues (S, T, and Y) that are amenable to phosphorylation. We then generated plasmids in which, in addition to the eight originally identified phosphosites, all sites of the high (11xA/F, 11xD/E) or any prediction score (16xA/F, 16xD/E) were mutated either to dephosphorylation mimetic (A/F) or phosphomimetic (D/E) residues. Expression of constructs in which phosphosites were mutated to dephosphorylation mimetics rescued ciliation rate indistinguishable from the wildtype motor, and only cells expressing 11xA/F showed a slightly but significantly reduced average cilium length (Figures 2B-2D). Expression of the phosphorylation mimetic constructs, in contrast, affected those phenotypes with expression of the 11xD/E and 16xD/E resulting in no ciliogenesis (Figures 2B-2D). This suggests that phosphorylation of KIF3A could regulate motor activity for ciliogenesis.

### KIF3A tail domain phosphorylation does not regulate heterodimeric kinesin-2 for ciliogenesis

It has been reported that bulky tags fused to the C-terminal tail domain of kinesins can interfere with their function.<sup>16</sup> Thus, combining a C-terminal mCherry-tag on KIF3B and mutations in the KIF3A tail domain could produce a non-predictable, combinatorial effect (synthetic effect). To exclude this possibility, we co-expressed the KIF3A constructs that did not rescue ciliogenesis (11xD/E and 16xD/E) with N-terminally HA- or HA-mCherry tagged KIF3B (Figure 3A). Indeed, while 16xD/E still did not rescue ciliogenesis, 11xD/E resulted in ciliogenesis at a level similar to wildtype KIF3A expression (Figures 3B-3D). Thus, the tagging position of KIF3B can produce synthetic effects with mutations in the KIF3A tail domain.

The five phosphosites that differ between the 11xD/E and 16xD/E are potential candidates for motor regulation. And indeed, the expression of a construct with only those five sites mutated (5xD/E) could also not rescue ciliogenesis (Figures 3B-3D). Thus, we next tested if mutating any of the five sites in the 5xD/E construct individually to phosphomimetic residues affected cilium generation. Only the expression of T627D and Y657E significantly reduced the ciliogenesis rate, while the expression of S651D and Y657E slightly but significantly reduced

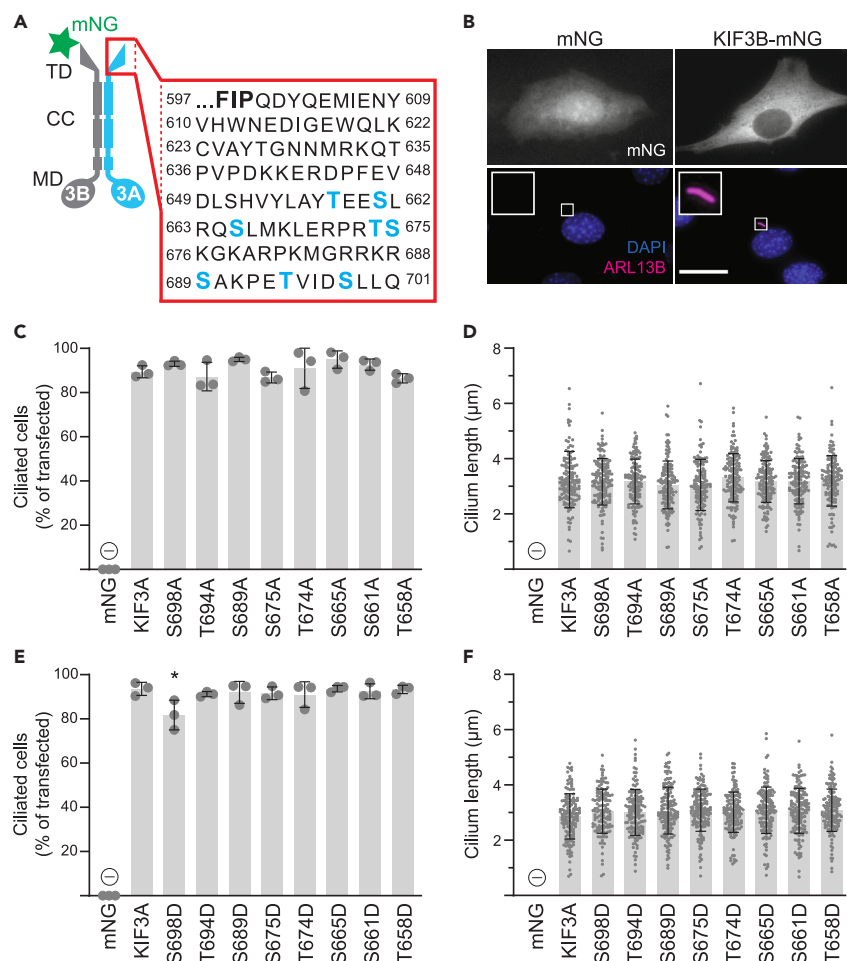


**Figure 1. Phosphorylation in the C-terminal half of the KIF3A tail has only minor effects on the ciliogenesis rate and average cilium lengths**

(A) Schematic of the heterodimeric KIF3A/KIF3B motor. KIF3A is shown in light blue, and the mNeonGreen-tagged (mNG) KIF3B subunit is shown in gray. For clarity, the kinesin-associated protein (KAP) is not shown. Letters in the red box show the amino acid sequence of the KIF3A tail in standard one-letter code, and small numbers denote residue numbers with respect to the full-length protein. The sequence ‘FIP’ (597–599, bold) marks the transition from the coiled-coil (CC) domain to the tail domain (TD), and potential phosphorylation sites, as chosen in ref.<sup>11</sup>, are shown in light blue. MD, motor domain.

(B–F) *Kif3a*<sup>-/-</sup>; *Kif3b*<sup>-/-</sup> 3T3 cells were co-transfected with an untagged KIF3A construct (WT or mutant), and KIF3B tagged with mNG (green) or control transfected with mNG (green). Subsequently, cells were serum-starved for two days to induce ciliogenesis and then fixed and stained with DAPI (blue) and an antibody against the ciliary membrane marker ARL13B (magenta). Scale bar, 20  $\mu\text{m}$ . (B) Representative images showing cells transfected with WT kinesin-2 or mNG. (C–F) Quantification of the percentage of transfected cells that generate a primary cilium (C, E) and average cilium length (D, F) when transfected with KIF3A constructs in which single phosphosites were mutated to the dephosphorylation mimetic residue alanine (A) (C, D) or phosphorylation mimetic residue aspartate (D) (E, F). One-way ANOVA revealed a significant difference in ciliation rate but not average cilium length between groups (C:  $F(9,20) = 150.7$ ,  $p < 0.001$ ; E:  $F(9,20) = 182.6$ ,  $p < 0.001$ ) but no difference in cilium length between groups (D:  $F(8,1267) = 1.3$ ,  $p = 0.25$ ; F:  $F(8,1316) = 1.2$ ,  $p = 0.31$ ). Groups that were significantly different from WT kinesin-2 according to Dunnett’s multiple comparison tests are labeled \* ( $p < 0.05$ ), and conditions in which ciliogenesis was completely blocked are labeled  $\emptyset$ . All data are from three independent experiments with  $n \geq 149$  transfected cells per condition and represented as mean  $\pm$  SD. Representative images of cellular phenotypes quantified in panels C–F are shown in Figure S1.

average cilium length (Figure 4). Since the effect on the ciliogenesis rate was more pronounced, we decided to focus on this phenotype. Thus, from all the potential phosphorylation sites in the KIF3A tail domain, individual phosphomimetic mutations of T627D, Y657E, as well as S698D (Figure 1E) significantly reduced the ciliogenesis rate.

It has been reported that phosphorylation of the KIF3A tail domain at multiple sites can cooperatively regulate motor binding to N-cadherin cargo complexes during intracellular transport.<sup>17</sup> Therefore, we tested if any combination of the three identified sites would synergistically reduce the ciliogenesis rate. While expression of the constructs combining the mutations T627D/S698D and Y657D/S698D reduced the ciliation rate moderately but significantly compared to wildtype KIF3A, expression of T627D/Y657E resulted in a complete lack of cilia (Figure 5). While the latter resulted in a strong phenotype, it is important to note that phosphomimetic residues do not mimic all features of the phosphorylated amino acids.<sup>18</sup> This is especially true for tyrosine (Y), which we mimicked with glutamate (E) for the lack

**Table 1. Potential phosphorylation sites in the KIF3A tail domain**

AA	Construct	NETphos 3.1		PhosphoMotif Finder <sup>13</sup>		
		Generic predict. score <sup>14</sup>	Specific prediction score <sup>15</sup>	Motif	Kinase/ Phosphatase	PMID
Y602	11xA/F, 11xD/E, 16xA/F, 16xD/E	N/A	0.586 (EGFR)	QDYQ	EGFR	8578591
			0.446 (INSR)	-	-	-
			-	DY	TC-PTP	11352902,12237455
Y609	Y609E, 5xD/E, 16xA/F, 16xD/E	N/A	0.391 (EGFR)	-	-	-
			-	ENY	SHP1	11994017
Y626	11xA/F, 11xD/E, 16xA/F, 16xD/E	0.563	0.415 (EGFR)	-	-	-
			0.398 (INSR)	-	-	-
			-	YT	SRC	16273072
T627	T627D, T627D/S698D, T627D/Y657E, T627N/Y657Q, T627D/Y657E/S698D, T627A/Y657F, 5xD/E, 16xA/F, 16xD/E	N/A	0.455 (GSK3)	-	-	-
			0.449 (CaM-II)	-	-	-
			0.402 (CDK1)	-	-	-
			0.396 (CKI)	-	-	-
			0.542 (p38MAPK)	-	-	-
T635	11xA/F, 11xD/E, 16xA/F, 16xD/E	0.992	0.448 (CDK5)	QTP	GSK3, ERK1,	16020478
			0.473 (PKG)	-	ERK2, CDK5	-
			0.466 (GSK3)	QTP	-	16020478
			0.457 (RSK)	-	GSK3, ERK1,	-
			0.443 (CaM-II)	RKQT	ERK2, CDK5	1956339
			-	KQT	-	1956339
			-	-	CaM-II, PKC, PKA PKA, PKC	-
S651	S651D, 5xD/E, 16xA/F, 16xD/E	N/A	0.453 (GSK3)	-	-	-
			0.450 (CaM-II)	-	-	-
			0.438 (CKII)	SHVpY	CKII	7735314
			0.422 (CDK1)	-	-	-
			0.418 (p38MAPK)	-	-	-
Y654	Y654E, 5xD/E, 16xA/F, 16xD/E	N/A	0.444 (SRC)	-	-	-
Y657	Y657E, Y657E/S698D, T627D/Y657E, T627N/Y657Q, T627D/Y657E/S698D, T627A/Y657F, 5xD/E, 16xA/F, 16xD/E	N/A	0.394 (INSR)	YT	SRC	16273072
T658	T658A, T658D, 8xA, 8xD, 11xA/F, 11xD/E, 16xA/F, 16xD/E	N/A	0.487 (CDK1)	-	-	-
			0.456 (GSK3)	-	-	-
			0.450 (CaM-II)	-	-	-
			-	TEES	CKI	12925738
S661	S661A, S661D, 8xA, 8xD, 11xA/F, 11xD/E, 16xA/F, 16xD/E	0.730	0.692 (PKC)	SLR	PKC, PKA	1956339
			0.518 (CKI)	SLRQSL	CKI	12925738
			0.467 (GSK3)	SLRQpS	GSK3	1956339
			0.427 (CaM-II)	-	-	-
			0.412 (DNAPK)	-	-	-
			-	ESLRQ	BARK	1645191
			-	SLRQS	MAPKAPK2	15629715
-	ESLRQS	GRK1	1645191			
S665	S665A, S665D, 8xA, 8xD, 11xA/F, 11xD/E, 16xA/F, 16xD/E	0.946	0.737 (PKA)	RQS	PKA, PKC	1956339
			0.556 (RSK)	-	-	-
			0.467 (GSK3)	-	-	-
			0.444 (CaM-II)	-	-	-
			0.428 (DNAPK)	-	-	-
			0.425 (CDK1)	-	-	-

(Continued on next page)

Table 1. Continued

AA	Construct	NETphos 3.1		PhosphoMotif Finder <sup>13</sup>		
		Generic predict. score <sup>14</sup>	Specific prediction score <sup>15</sup>	Motif	Kinase/ Phosphatase	PMID
T674	T674A, T674D, 8xA, 8xD, 11xA/F, 11xD/E, 16xA/F, 16xD/E	0.979	0.461 (GSK3) 0.441(CaM-II) 0.431 (PKG) 0.430 (PKC) – –	– LERPRTSK- RPRT LERPRT LERPRT	– CaM-II – PKC, CaM-II CHK1 CaM-IV	– 8280084 – 1956339- 10648819 9452427
S675	S675A, S675D, 8xA, 8xD, 11xA/F, 11xD/E, 16xA/F, 16xD/E	0.996	0.596 (PKC) 0.471 (GSK3) 0.467 (CaM-II) 0.411 (CKI) 0.411 (PKA) 0.398 (RSK) –	RPRTSK – – – RTS, TSK – TSKGKA	PKC – – – PKA, PKC – GRK1	1956339 – – – 1956339 – 1645191
S689	S689A, S689D, 8xA, 8xD, 11xA/F, 11xD/E, 16xA/F, 16xD/E	0.996	0.794 (PKA) 0.718 (PKG) 0.563 (PKC) 0.444 (CaM-II) 0.439 (GSK3) 0.435 (RSK) 0.416 (CDK1) – –	RKRS, SAK – RKRS RKRS – – – RRKRS RRKRS	PKA, PKC – PKC CaM-II – – – ZIP PIM1	1956339 – 1956339 16273072 – – – 15001356 1416988
T694	T694A, T694D, 8xA, 8xD, 11xA/F, 11xD/E, 16xA/F, 16xD/E	N/A	0.446 (GSK3) 0.428 (CaM-II) – – – – –	– – KPET ETVID ETVIDS TVID TVIDSL	– – PKA, PKC BARK GRK1 CKII CKI	– – 1956339 1645191 1645191 2044770, 2117608, 7735314, 9272871 12925738
S698	S698A, S698D, T627D/S698D, Y657E/S698D, T627D/Y657E/S698D, 8xA, 8xD, 11xA/F, 11xD/E, 16xA/F, 16xD/E	N/A	0.462 (GSK3) 0.454 (CaM-II) 0.418 (CKII) 0.401 (PKA) 0.398 (CKI)	– – – – –	– – – – –	– – – – –

Abbreviations used in table: N/A, not applicable (no generic score generated); AA, amino acid; EGFR, epidermal growth factor receptor; INSR, insulin receptor; GSK3, glycogen synthase kinase-3; CaM-(II,IV), calmodulin-dependent protein kinase (II,IV); CDK(1,5), cyclin-dependent protein kinase-(1,5); CK(I,II), casein kinase (I,II); p38MAPK, p38 mitogen-activated protein kinase; PK(G/C/A), protein kinase (G/C/A); RSK, ribosomal s6 kinase; SRC, Src family kinase; DNAPK, DNA-dependent protein kinase; TC-PTP, T-cell protein tyrosine phosphatase; SHP1, Src, homology region 2 domain-containing phosphatase-1; ERK(1,2), extracellular signal-regulated kinase-(1,2); BARK,  $\beta$ -adrenergic receptor kinase; MAPKAPK2, MAP kinase-activated protein kinase 2; GRK1, G protein-coupled receptor kinase 1; CHK1, checkpoint kinase 1; ZIP, zipper-interacting protein kinase; PIM1, Pim1 kinase.

of a better phosphomimetic residue. It is thus possible that incorporating dissimilar residues rather than a physiological role of phosphorylation exerted the observed effect on ciliogenesis. To test this possibility, we mutated T627 to asparagine (N) and Y657 to glutamine (Q). (N) and (Q) are structurally similar to (D) and (E) but do not contain the phosphomimetic negative charge. Importantly, expression of the T627N/Y657Q construct also did not rescue ciliogenesis. These results suggest that the T627 and Y657 play an important role in the ciliogenesis function of kinesin-2 but are not regulated via phosphorylation.

In the experiments reported thus far, we employed serum starvation to induce a high rate of ciliogenesis. *In vivo*, cilia dynamically assemble in the G<sub>1/0</sub>-phase and disassemble during the transition to the M-phase of the cell cycle.<sup>19</sup> To confirm that our results are not specific to the artificial serum starvation state but reflect a physiological condition, we repeated key experiments in cycling cells grown in full medium supplemented with 10% serum. As expected, the average ciliation rate driven by WT kinesin-2 fell from over 80% to around 30%, and the average

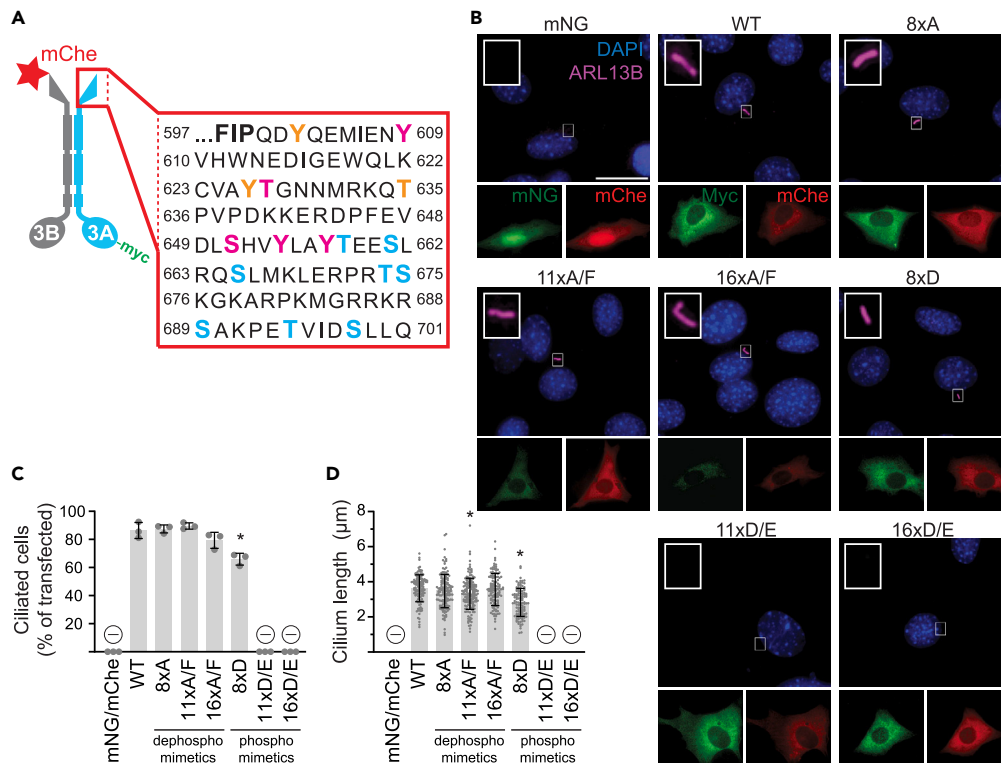


**Figure 2. Mutation of further potential phosphorylation site groups suggests that phosphorylation may regulate kinesin-2 for ciliogenesis**

(A) Schematic of the heterodimeric kinesin-2 motor shown similarly as in Figure 1A. In this experiment, the KIF3A subunit was visualized with a myc-tag (green), and the KIF3B subunit with C-terminal mCherry-tag (mCherry; red). All potential phosphorylation sites mutated to dephosphorylation mimetic residues (A/F) or phosphomimetic residues (D/E) are indicated. The residues mutated in the constructs 8xA and 8xD are shown in light blue. The additional residues mutated in 11xA/F and 11xD/E are shown in orange, and further additional mutated residues in the constructs 16xA/F and 16xD/E are shown in magenta.

(B–D) *Kif3a*<sup>-/-</sup>; *Kif3b*<sup>-/-</sup> 3T3 cells were co-transfected with the indicated plasmids, serum-starved for two days, and then fixed and stained. (B) Representative images of *Kif3a*<sup>-/-</sup>; *Kif3b*<sup>-/-</sup> 3T3 cells expressing either soluble mNeonGreen (mNG; green) and mCherry (red) or myc-tagged KIF3A (WT or mutants; green) and KIF3B-mCherry (red). Cells are stained with DAPI (blue) and an antibody to ARL13B (magenta). Scale bar, 20 µm. (C–D) Quantification of the ciliogenesis rescue rate (C) and mean cilium lengths (D). One-way ANOVA revealed a significant difference in ciliation rates between groups ( $F(7,16) = 459.9$ ,  $p < 0.001$ ) and a significant difference in cilium length between groups ( $F(4,667) = 16.3$ ,  $p < 0.001$ ). Groups that were significantly different from WT kinesin-2 according to Dunnett's multiple comparison tests are labeled \* ( $p < 0.05$ ), and conditions in which ciliogenesis was completely blocked are labeled  $\emptyset$ . All data are from three independent experiments with  $n \geq 150$  transfected cells per condition and represented as mean  $\pm$  SD.

cilium length fell from over 3 µm to about 2 µm in serum-starved versus cycling cells (Figures 2B–2D and 6A–6C). Importantly, a newly generated dephosphomimetic construct, T627A/Y657F, as well as the previously tested grouped dephosphomimetic constructs 8xA and 16xA rescued ciliogenesis rates and cilium length comparable to WT motor in cycling cells (Figure 6). Additionally, constructs that could not rescue ciliogenesis in serum-starved cells (the phosphomimetic 16xD/E as well as T627D/Y657E and T627N/Y657Q) could also not rescue ciliogenesis in cells incubated in full medium. However, whereas the 8xD, T627D, and Y657E phosphomimetic mutants showed a slight impairment of ciliogenesis rescue in serum-starved cells (Figures 2C and 4C), they were not different from WT motor in cycling cells in full medium (Figures 6B and 6E). Regarding cilium length, of the three constructs, only 8xD and Y657 in serum-starved cells (Figures 2D and 4D) and Y657 in cycling cells (Figures 6C and 6F) measured slightly but significantly shorter than WT cilia.

Thus, in summary, we conclude that T627 and Y657 are important residues for heterodimeric kinesin-2 function during ciliogenesis. However, phosphorylation of these residues (or introduction of negative charge at those sites) does not regulate this motor for cilium assembly and maintenance in serum-starved and cycling cultured murine fibroblasts.

## DISCUSSION

IFT is essential for cilium assembly, maintenance, and function, and its dysfunction can cause ciliopathies. The regulation of IFT, especially via phosphorylation, is of interest because kinases and phosphatases are druggable targets and could provide potential strategies to alleviate ciliopathies.<sup>20–22</sup> Ciliogenesis rate, cilium length, and/or cilium signaling function, all of which are frequently altered in disease states, can be regulated by kinases and phosphatases.<sup>6,22</sup> However, it has been challenging to identify ciliary kinase targets and delineate the function of phosphorylation on those targets. Kinesin-2 directly drives ciliogenesis, making it a potential target of ciliogenesis regulation, including by

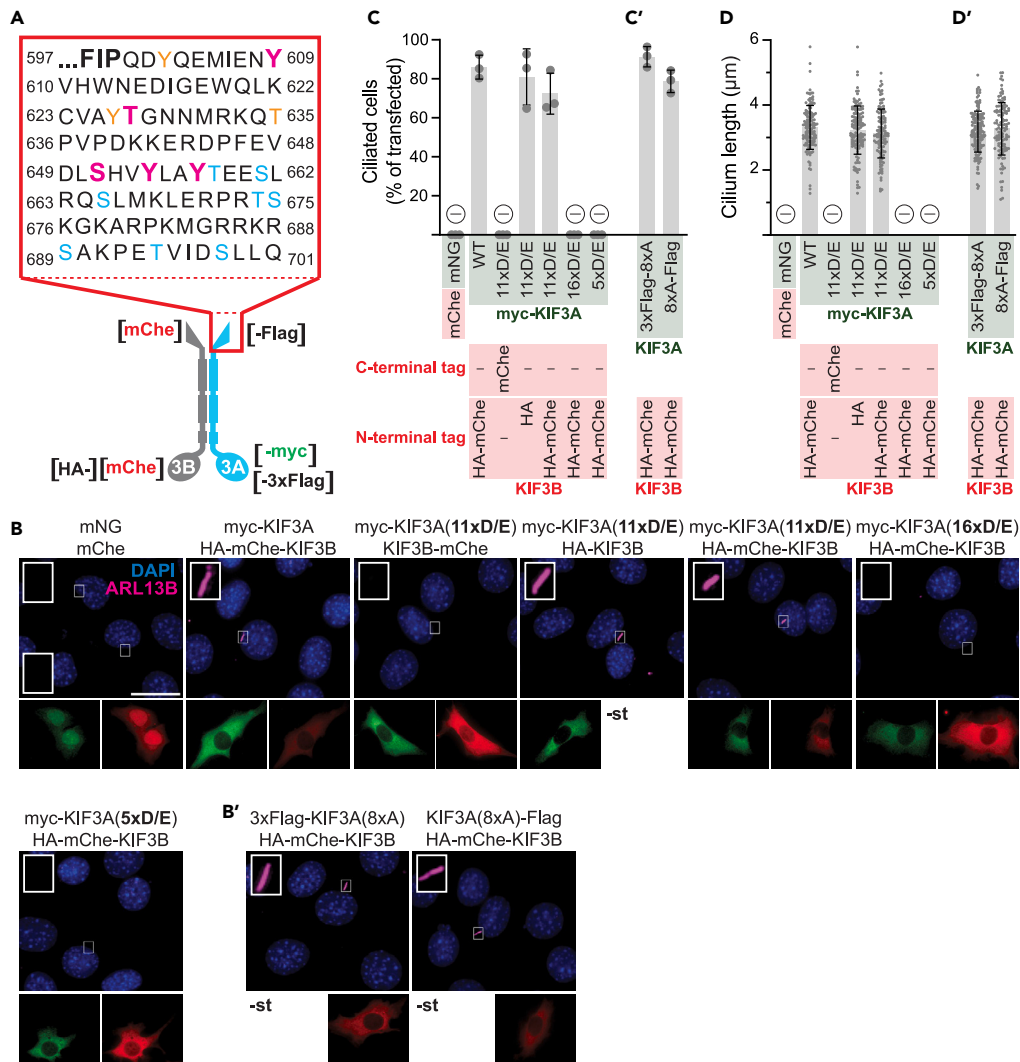


**Figure 3. The position and the identity of the visualization tag influence kinesin-2 function**

(A) Schematic of the heterodimeric kinesin-2 motor with color coding of potential phosphorylation sites as in Figure 2A. All tagging sites on the KIF3A and KIF3B subunits are indicated.

(B–D) To evaluate the effect of tagging on KIF3B (B–D) and KIF3A (B'–D'), *Kif3a*<sup>-/-</sup>; *Kif3b*<sup>-/-</sup> 3T3 cells were co-transfected with the indicated plasmids, serum-starved for two days, and then fixed and stained. (B) Representative images of cells expressing the indicated proteins. Nuclei were stained with DAPI (blue), cilia were visualized with an antibody to ARL13B (magenta), and no staining for the HA- and Flag-tags (-st) was performed. Scale bar, 20  $\mu$ m. (C–D) Quantification of the ciliation rates (C and C') and average cilium lengths (D and D') in cells expressing the indicated proteins. One-way ANOVA revealed a significant difference in ciliation rates between groups ( $F(8,18) = 122.6$ ,  $p < 0.001$ ) but no difference in cilium length between groups ( $F(4,664) = 1.3$ ,  $p = 0.25$ ). Conditions in which ciliogenesis was completely blocked are labeled  $\emptyset$ . All data are from three independent experiments with  $n \geq 150$  transfected cells per condition and represented as mean  $\pm$  SD.

phosphorylation. In turn, because kinesin-2 activity is so closely tied to ciliogenesis rate and cilium function, identifying intracellular signaling pathways that regulate its activity would be of pharmacological interest, especially since there are no direct, specific inhibitors for most kinesin motors.<sup>23,24</sup>

### Dephosphorylation mimetic mutations of eight potential phosphorylation sites in the KIF3A tail domain do not impair ciliogenesis as previously reported

Chaya et al., who identified KIF3A as an essential target of CILK1, mapped the primary CILK1 phosphorylation site on KIF3A to T674. They found that an RNAi-resistant T674A expression construct rescued ciliogenesis even more effectively than the wildtype motor in KIF3A RNAi-treated cells. However, a construct with all eight potential CILK1 phosphorylation sites mutated to dephosphorylation mimetic alanines

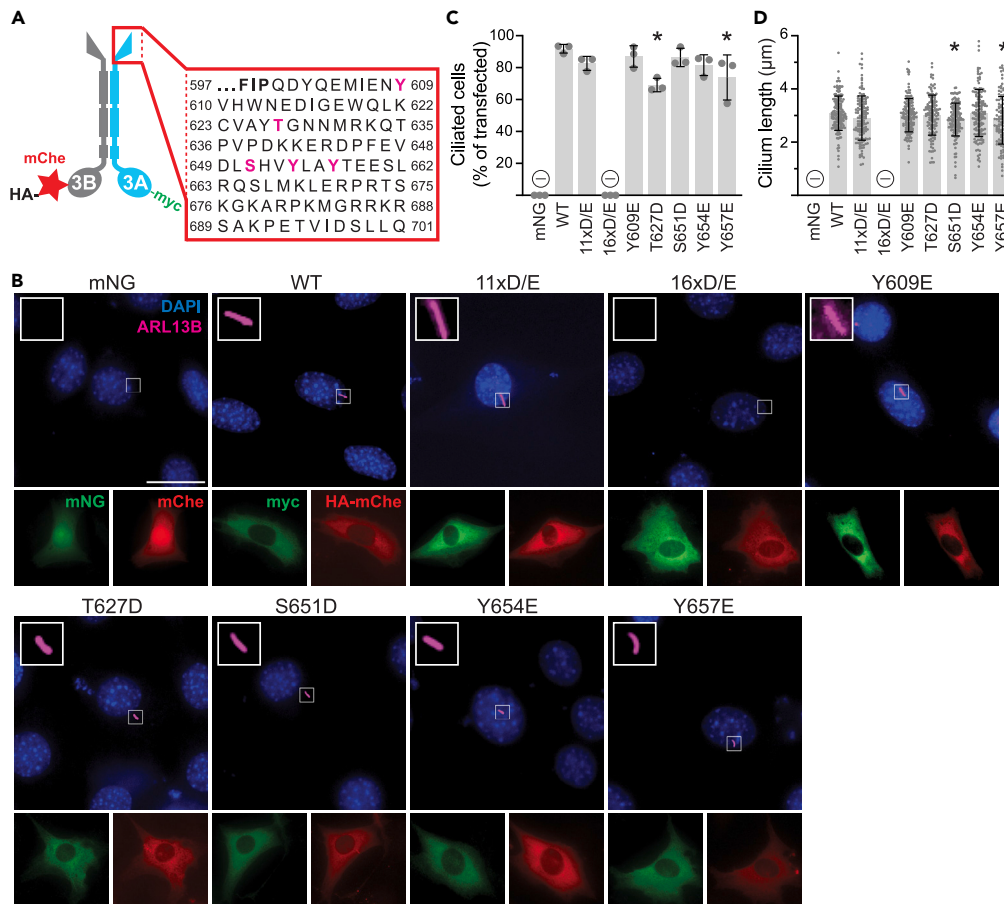


**Figure 4. Phosphorylation of two individual residues in the N-terminal part of the KIF3A tail modestly reduces cilium length and ciliogenesis rate**  
(A) Schematic of the heterodimeric kinesin-2 motor with magenta-colored letters indicating amino acids that make up the difference between the 16xD/E and 11xD/E groups.  
(B–D) *Kif3a*<sup>-/-</sup>; *Kif3b*<sup>-/-</sup> 3T3 cells were co-transfected with the indicated plasmids, serum-starved for two days, and then fixed and stained. (B) Representative images of cells co-transfected with the indicated KIF3A mutations (green) and HA-mChe-KIF3B (red). Nuclei were stained with DAPI (blue), and cilia were visualized with an antibody to ARL13B (magenta). Scale bar, 20 μm. (C–D) Quantification of the percentage of transfected cells that generate a primary cilium (C) and the average cilium length (D). One-way ANOVA revealed a significant difference in ciliation rates between groups ( $F(8,18) = 100.1$ ,  $p < 0.001$ ) and a significant difference in cilium length between groups ( $F(6,1001) = 3.1$ ,  $p < 0.01$ ). Groups that were significantly different from WT kinesin-2 according to Dunnett's multiple comparison tests are labeled \* ( $p < 0.05$ ), and conditions in which ciliogenesis was completely blocked are labeled  $\emptyset$ . All data are from three independent experiments with  $n \geq 150$  transfected cells per condition and represented as mean  $\pm$  SD.

(8xA) failed to rescue ciliogenesis.<sup>11</sup> Inspired by these findings, we set out to delineate which of the eight reported sites negatively regulates the kinesin-2 motor for ciliogenesis when phosphorylated. To our surprise, re-expression of KIF3A in which we mutated single sites or all eight sites (8xA) to dephosphorylation mimetic alanines rescued ciliogenesis indistinguishable from wildtype-expressing cells in both starved and cycling cells (Figures 1C, 1D, 2C, 2D, and 6A–6C). While Chaya et al. relied on RNAi-mediated *Kif3a* knockdown and re-expression of RNAi-resistant expression constructs in 3T3 cells, we utilized a well-characterized *Kif3a*<sup>-/-</sup>; *Kif3b*<sup>-/-</sup> double-knockout cell line that was also derived from 3T3 cells.<sup>11,12</sup> Since we used the same cell type, the disparity in our results does not likely stem from differential cell-type regulation. It may originate from the method used to deplete endogenous KIF3A or the constructs to rescue KIF3A expression. Furthermore, we used an antibody directed against the ciliary membrane protein ARL13B to detect cilia, while Chaya et al. stained with an anti-acetylated tubulin antibody to detect the axonemal microtubules. It is theoretically possible that expression of the 8xA construct rescues ciliogenesis but reduces acetylation of the axonemal microtubules, preventing the detection of cilia with an antibody directed against acetylated tubulin. However, we think that this scenario is unlikely. To visualize KIF3A for immunohistochemistry, we used a myc-tag N-terminally fused to the motor domain, whereas Chaya et al. used a FLAG tag.<sup>11</sup> To control for this, we compared ciliogenesis rates of cells re-expressing various Flag-tagged and myc-tagged constructs (Figures 3B'–3D'). Since expression of the differently tagged KIF3A constructs resulted in similar ciliation rates and lengths, these experiments ruled out differential tagging as a cause for the disparate results. This suggests the method employed to deplete KIF3A in the parental 3T3 cells as the probable origin for the different observations. While the knockout cells do not produce any cilia, *Kif3a*

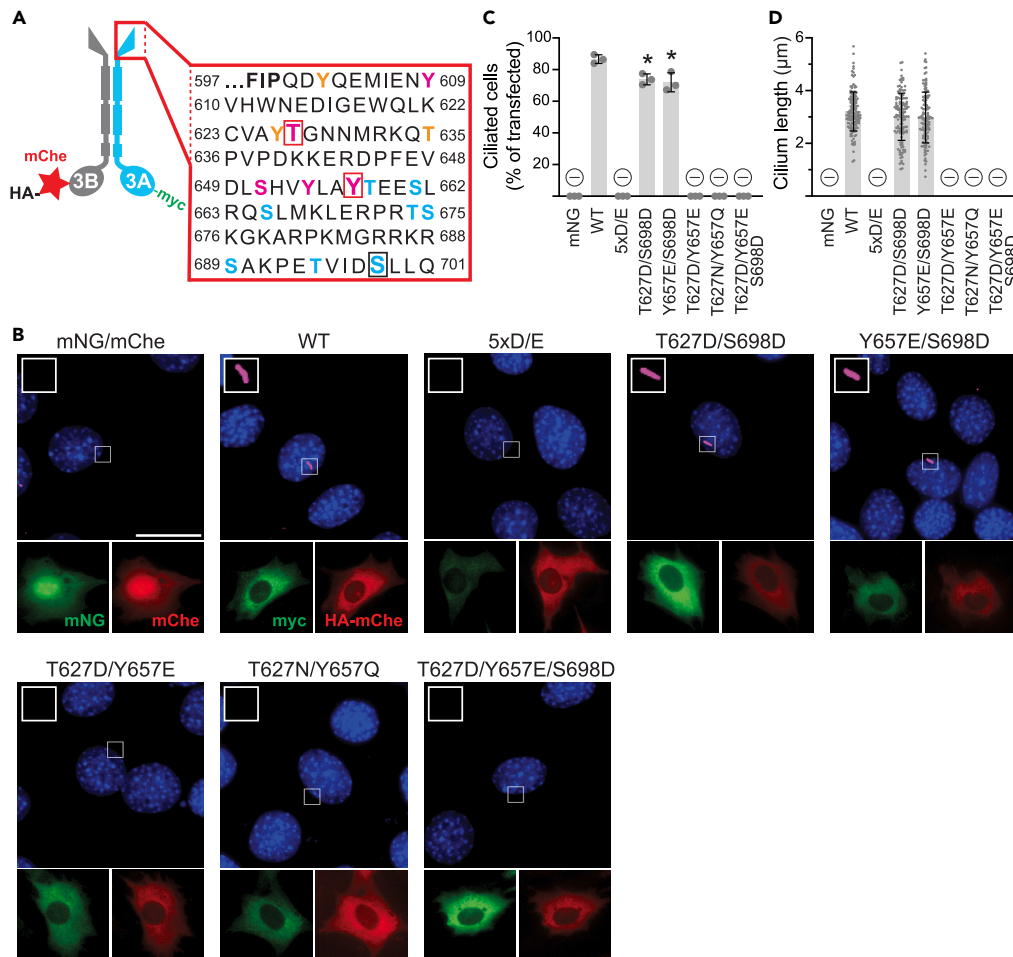


**Figure 5. KIF3A tail domain phosphorylation does not regulate the kinesin-2 motor for ciliogenesis in starvation conditions in mouse embryonic fibroblasts**

(A) Schematic of the heterodimeric kinesin-2 motor with color coding as in Figures 2 and 3. Mutated phosphosites that have no synergistic (black box) or have a synergistic effect (red box) on ciliogenesis are indicated.

(B–D) *Kif3a*<sup>-/-</sup>; *Kif3b*<sup>-/-</sup> 3T3 cells were co-transfected with the indicated plasmids, serum-starved for two days, and then fixed and stained. (B) Representative images of cells co-transfected with mNG (green) and mChe (red) or the indicated KIF3A mutations (green) and HA-mChe-KIF3B (red). Nuclei were stained with DAPI (blue), and cilia were visualized with an antibody to ARL13B (magenta). Scale bar, 20  $\mu\text{m}$ . (C–D) Quantification of the percentage of transfected cells that generate a primary cilium (C) and the average cilium length (D). One-way ANOVA revealed a significant difference in ciliation rates between groups ( $F(7, 16) = 701.0$ ,  $p < 0.001$ ) but no difference in cilium length between groups ( $F(2, 405) = 2.9$ ,  $p = 0.06$ ). Groups that were significantly different from WT kinesin-2 according to Dunnett's multiple comparison tests are labeled \* ( $p < 0.05$ ), and conditions in which ciliogenesis was completely blocked are labeled  $\emptyset$ . All data are from three independent experiments with  $n \geq 150$  transfected cells per condition and represented as mean  $\pm$  SD.

RNAi reduced, but did not abolish ciliogenesis. Similarly, re-expression of wildtype *Kif3a* in knockout cells completely rescued ciliogenesis, while ciliogenesis was increased, but not restored in cells with *Kif3a* RNAi. Thus, as expected, rescue in the knockout cells produced more robust results than using RNAi, leaving the method for KIF3A depletion as the most likely source of the observed differences.

Another study, Gailey et al., was also unable to confirm the claim of Chaya et al. that CILK1 regulates IFT via KIF3A phosphorylation, supporting our data.<sup>25</sup> In contrast to *CILK1*<sup>-/-</sup> mice, they found that *KIF3A(T674A)* mice are healthy, and fibroblasts derived from this model had normal ciliogenesis rates and merely displayed 8% longer cilia. This finding suggests that CILK1 regulates IFT via other targets. In agreement with Gailey et al., we observed a cilium length increase in cells expressing *KIF3A(T674A)*, which was in our system not statistically significant, however.

The phosphorylation of T674 by CILK1 has been demonstrated independently by three groups.<sup>11,26,27</sup> It is thus important to point out that we are not challenging this phosphorylation event but instead report that phosphorylation of eight potential phosphorylation sites in the tail domain of KIF3A, including T674, does not regulate the motor for its function in ciliogenesis. It is possible, however, that KIF3A phosphorylation on T674 regulates kinesin-2 for another transport process.

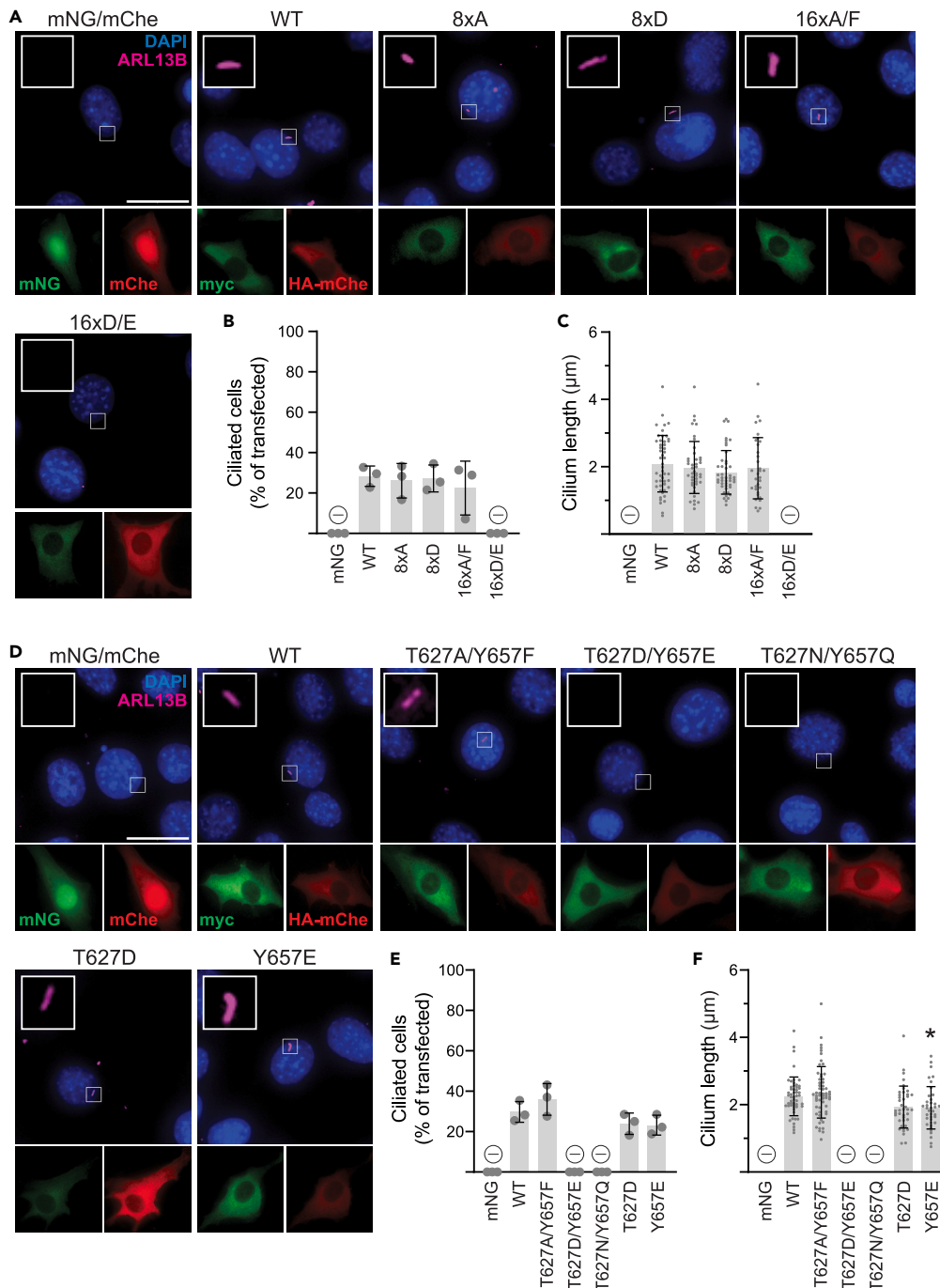


**Figure 6. KIF3A tail domain phosphorylation does not regulate the kinesin-2 motor for ciliogenesis in physiological conditions in mouse embryonic fibroblasts**

*Kif3a*<sup>-/-</sup>; *Kif3b*<sup>-/-</sup> 3T3 cells were co-transfected with the indicated plasmids driving expression of KIF3A with phosphomimetic mutations either in large groups encompassing many sites (A-C) or one or two mutations (D-F), allowed to grow for two days in normal media, and then fixed and stained.

(A and D) Representative images of cells co-transfected with mNG (green) and mChe (red) or the indicated KIF3A mutations (green) and HA-mChe-KIF3B (red). Nuclei were stained with DAPI (blue), and cilia were visualized with an antibody to ARL13B (magenta). Scale bar, 20  $\mu\text{m}$ .

(B, C, E, and F) Quantification of the percentage of transfected cells that generate a primary cilium (B, E) and the average cilium length (C, F). In the constructs in which many sites had been mutated, one-way ANOVA revealed a significant difference in ciliation rates between groups (B:  $F(5,12) = 10.35$ ,  $p < 0.001$ ) but no

**Figure 6. Continued**

difference in cilium length (C:  $F(3,166) = 0.82, p = 0.48$ ). In the constructs with only one or two mutations, one-way ANOVA revealed a significant difference in ciliation rates (E:  $F(6,14) = 36.72, p < 0.001$ ) and in cilium length (F:  $F(3,186) = 5.73, p < 0.001$ ). Groups that were significantly different from WT kinesin-2 according to Dunnett's multiple comparison tests are labeled \* ( $p < 0.05$ ), and conditions in which ciliogenesis was completely blocked are labeled  $\emptyset$ . All data are from three independent experiments with  $n \geq 150$  transfected cells per condition and represented as mean  $\pm$  SD.

**The position of the visualization tag influences kinesin-2 function**

It has been demonstrated that globular tags can interfere with kinesin function. Fusion of mCitrine to the tail domain of KIF17 partially interfered with autoinhibition, priming the motor for activation.<sup>16</sup> Additionally, we found that introducing several negatively charged residues into the tail region of KIF3A (8xD, 11xD/E, and 16xD/E) reduced the ability of kinesin-2 to drive ciliogenesis. Thus, we reasoned that the fusion of the highly negatively charged FLAG tag to the KIF3A tail domain might have the same effect.

Here, we investigated how the position and charge of the visualization tag on the KIF3A and KIF3B subunits affect kinesin-2 function. Specifically, we fused a charged FLAG tag and a bulky mCherry-tag to the N- and C- termini of KIF3A and KIF3B, respectively, and measured the effect on ciliogenesis. We did this experiment in a context where potentially sensitizing phosphomimetic mutations were introduced into the KIF3A tail. We neither observed an effect of fusing 3xFlag to the N-terminus nor fusing Flag to the C-terminus of KIF3A(8xA). However, co-expression of N- or C-terminally mCherry tagged KIF3B with KIF3A-11xD/E had opposing effects. While the N-terminally tagged construct rescued ciliogenesis close to wildtype levels, C-terminally tagging abolished ciliogenesis (Figure 3). These findings were surprising since C-terminally mCherry tagged KIF3B fully recovers ciliogenesis when expressed in combination with wildtype KIF3A without sensitizing mutations.<sup>12</sup> Our results serve as a reminder that the position of the visualization tag should be carefully considered for kinesin motors used in functional studies.

**Implications for the differential regulation of kinesin-2 activity for specific intracellular transport processes**

In this study, we examined whether phosphorylation of the KIF3A tail domain regulates the kinesin-2 holoenzyme for ciliogenesis. We mutated all potential phosphorylation sites in the KIF3A tail domain and assessed the effect on the ciliogenesis rate and average cilium length, both of which are frequently altered in human disease. We conducted most experiments with cells cultured in starvation medium (1% serum), which is a common method to induce high rates of ciliogenesis. However, cycling cells also ciliate spontaneously, albeit at a lower frequency.<sup>19</sup> Since the internal activity of signal transduction pathways and thus the potential for KIF3A phosphorylation differ greatly in cycling and serum-starved cells,<sup>28,29</sup> we conducted key experiments in cycling cells grown in full medium. Importantly, in both conditions, the same set of dephosphomimetic constructs rescued ciliogenesis, albeit with lower frequency in serum-deprived cells, as expected. Similarly, the grouped phosphomimetic constructs that could not rescue ciliogenesis in serum-starved cells also did not produce cilia in cycling cells. These findings indicate that our results are broadly applicable and not specific to the potentially non-physiological serum-starved state. We did observe that several constructs that exhibited a slight impairment in rescuing ciliogenesis rates in serum-starved cells did not show the same difference in cycling cells, further corroborating the notion that kinesin-2 is not regulated via phosphorylation of those residues under physiological conditions.

Examining all potential phosphorylation sites in the KIF3A tail domain, we found two single-site phosphomimetic substitutions, S651D and Y657E, that significantly reduced the average cilium length compared to wildtype kinesin-2 expressing cells. However, the resulting cilium length reduction was less than 10% of the wildtype length, and the biological significance is thus uncertain. For the ciliogenesis rate, we obtained much more pronounced results. Introducing two phosphomimetic mutations at T627, a potential glycogen synthase kinase-3 or calmodulin-dependent kinase-II target, and Y657, a potential insulin receptor or Src family kinase target, abolished ciliogenesis in both serum-starved and cycling cells. However, mutating those sites to amino acids with similar side chains to (D) and (E) but without the phosphomimetic negative charge, i.e., T627N and Y657Q, phenocopied the phosphomimetic mutations. Kinesin tails mainly comprise intrinsically disordered regions (IDRs),<sup>30</sup> thought to be involved in cargo binding. Aromatic residues within the IDRs, such as Y, substantially contribute to protein-protein interactions.<sup>31</sup> It is conceivable that changing the biochemical properties of amino side chains in the IDRs, especially those of aromatic residues, could abolish IDR function. Thus, we believe that T627 and Y657 are functionally important for the kinesin-2 motor. However, the observed effect on ciliogenesis at these sites is caused by introducing side chains with different biochemical properties, such as aromaticity and polarity, and does not depend on the phosphomimetic negative charge. In summary, these results demonstrate that phosphorylation of the KIF3A tail domain does not regulate the kinesin-2 holoenzyme for ciliogenesis.

Even though initially deemed unlikely, mammalian kinesin-2 may be regulated for IFT similarly to its *C. reinhardtii* homolog kinesin-II via the KIF3B subunit, a possibility we will explore in future work. This notion agrees with the observation that many aspects of mammalian IFT show more conservation with *C. reinhardtii* than with more closely related species, such as *C. elegans*.<sup>12,32</sup> Subunit- or domain-specific phosphorylation effects could explain how a motor protein like kinesin-2 can be differentially regulated for specific cargos in different transport processes. The transport of N-Cadherin<sup>17</sup> and the modulation of Hedgehog signaling<sup>33</sup> could be achieved via KIF3A tail domain phosphorylation, while bulk IFT could be regulated via KIF3B tail domain phosphorylation. Therefore, we believe a mechanism where single-site phosphorylation generally regulates kinesin-2 activity similarly for all cargo, as proposed by Phang et al., is unlikely.<sup>34</sup>

Since cellular signaling pathways can influence ciliogenesis and cilium length, several aspects of IFT, such as IFT train injection into the cilium, are most likely regulated by cell signaling.<sup>35,36</sup> However, cellular signaling pathways might not directly target kinesin-2. It is generally believed that cargo binding can suffice for kinesin activation.<sup>37</sup> Thus, regulation of IFT train availability or regulation of cargo binding via

post-translational modification of the cargo would allow kinesin-2 activation in a cargo-specific manner. Furthermore, some aspects of IFT, such as cargo release by kinesin-2 at the cilium tip, might not require regulation. A recent study elegantly showed that blocking IFT mid-cilium via a microfabricated wedge was sufficient to trigger spontaneous IFT reversal.<sup>38</sup> The authors suggested that derailing the IFT trains might be enough to trigger an intrinsic IFT train disassembly program that also leads to releasing the anterograde motor.

In summary, whether and how IFT motors are regulated is under active investigation. We report that phosphorylation of the KIF3A tail domain is dispensable for regulating the kinesin-2 holoenzyme for ciliogenesis. More work is required to discern whether kinesin-2 is directly or indirectly controlled for IFT and ciliogenesis and by what mechanism. A mechanistic understanding of this regulation has the potential to inform novel avenues to alleviate ciliopathies.

### Limitations of the study

We have demonstrated that in mouse embryonic fibroblasts, the phosphorylation status of the KIF3A tail domain does not regulate heterodimeric kinesin-2 for ciliogenesis or ciliary length. The cell type we use has a male karyotype, but since we are studying fundamental processes in motor function and ciliogenesis and these mechanisms are found in all cells, we have no reason to expect differences based on sex. We mutated potential phosphorylation sites to dephosphorylation and phosphorylation mimetics and thus did not directly look at phosphorylation. Except for two sites, also affected by mutations not introducing negative charge, we do not see an effect of these mutations on kinesin-2 function in ciliogenesis, and thus are confident that our main conclusion holds. However, our results are specific to the cell line used, and even though the core IFT machinery is conserved between tissues and even across species, there might be subtle differences in other cells. Lastly, we used immunostaining against the ciliary membrane protein ARL13B to detect cilia, reporting that the gross ciliary structure was intact. Our data do not reveal possible defects in ciliary microstructure or function, which needs to be addressed in future work.

### STAR★METHODS

Detailed methods are provided in the online version of this paper and include the following:

- [KEY RESOURCES TABLE](#)
- [RESOURCE AVAILABILITY](#)
  - Lead contact
  - Materials availability
  - Data and code availability
- [EXPERIMENTAL MODEL AND STUDY PARTICIPANT DETAILS](#)
- [METHOD DETAILS](#)
  - Bioinformatic analysis
  - Expression plasmids
  - Cell culture techniques, immunofluorescence, and microscopy
  - Microscopy and image analysis
- [QUANTIFICATION AND STATISTICAL ANALYSIS](#)

### SUPPLEMENTAL INFORMATION

Supplemental information can be found online at <https://doi.org/10.1016/j.isci.2024.109149>.

### ACKNOWLEDGMENTS

We want to thank Vrailas-Mortimer, A (Oregon State University) for helpful comments on the manuscript and the students from the Fall 2020 BSC 353 biotechnology class at Illinois State University (Abella, EK; Barsoum, A; Burkhart, J; Eshun, AA; Frakes, R; Goben, CE; Hafner, AW; Henderson, EC; Hudson, H; Krigbaum, JR; Lambaria, NS; Livingston, B; Patel, KR; Pauline, M; Ramirez, SG; Vargas, A.) for cloning the individual phosphomimetic KIF3A expression constructs. The cell line *Kif3a*<sup>-/-</sup>; *Kif3b*<sup>-/-</sup> 3T3 cells and the plasmids pmNeonGreen-N1, pmCherry-N1, MmKIF3B-mCherry, MmKIF3A were gifts from Verhey, KJ (University of Michigan Medical School). This work was supported by the National Institute of General Medical Sciences of the National Institutes of Health under award numbers R15GM137248 (to M.F.E.) and R35GM147641 (to M.F.E.), an internal Illinois State University grant to M.F.E. (URG-NFIG) and an internal Weigel Grant to A.S.F. The content is solely the authors' responsibility and does not necessarily represent the official views of the National Institutes of Health.

### AUTHOR CONTRIBUTIONS

M.F.E. conceptualized the study. A.S.F. performed the experiments. A.S.F. and J.M.A. analyzed the data. A.S.F. created the display items with input from all authors. M.F.E. wrote the article with input from all authors. Resources were provided from funding to M.F.E.

### DECLARATION OF INTERESTS

The authors declare no competing interests.

## DECLARATION OF GENERATIVE AI AND AI-ASSISTED TECHNOLOGIES IN THE WRITING PROCESS

ChatGPT ([openai.com](https://openai.com)) was used for an initial draft of the Discussion section. After using this tool, the authors reviewed and edited the content and take full responsibility for the content of the publication.

Received: July 14, 2023

Revised: November 21, 2023

Accepted: February 1, 2024

Published: February 5, 2024

## REFERENCES

1. Mill, P., Christensen, S.T., and Pedersen, L.B. (2023). Primary cilia as dynamic and diverse signalling hubs in development and disease. *Nat. Rev. Genet.* 24, 421–441. <https://doi.org/10.1038/s41576-023-00587-9>.
2. Lechtreck, K.F. (2015). IFT-Cargo Interactions and Protein Transport in Cilia. *Trends Biochem. Sci.* 40, 765–778. <https://doi.org/10.1016/j.tibs.2015.09.003>.
3. Pigino, G. (2021). Intraflagellar transport. *Curr. Biol.* 31, R530–R536. <https://doi.org/10.1016/j.cub.2021.03.081>.
4. Webb, S., Mukhopadhyay, A.G., and Roberts, A.J. (2020). Intraflagellar transport trains and motors: Insights from structure. *Semin. Cell Dev. Biol.* 107, 82–90. <https://doi.org/10.1016/j.semcdb.2020.05.021>.
5. Mul, W., Mitra, A., and Peterman, E.J.G. (2022). Mechanisms of Regulation in Intraflagellar Transport. *Cells* 11, 2737. <https://doi.org/10.3390/cells11172737>.
6. Reiter, J.F., and Leroux, M.R. (2017). Genes and molecular pathways underpinning ciliopathies. *Nat. Rev. Mol. Cell Biol.* 18, 533–547. <https://doi.org/10.1038/nrm.2017.60>.
7. Keeling, J., Tsiokas, L., and Maskey, D. (2016). Cellular Mechanisms of Ciliary Length Control. *Cells* 5, 6. <https://doi.org/10.3390/cells5010006>.
8. Wang, L., and Dynlacht, B.D. (2018). The Regulation of Cilium Assembly and Disassembly in Development and Disease. *Development* 145. <https://doi.org/10.1242/dev.151407>.
9. Liang, Y., Pang, Y., Wu, Q., Hu, Z., Han, X., Xu, Y., Deng, H., and Pan, J. (2014). FLA8/KIF3B Phosphorylation Regulates Kinesin-II Interaction with IFT-B to Control IFT Entry and Turnaround. *Dev. Cell* 30, 585–597. <https://doi.org/10.1016/j.devcel.2014.07.019>.
10. Funabashi, T., Katoh, Y., Okazaki, M., Sugawa, M., and Nakayama, K. (2018). Interaction of heterotrimeric kinesin-II with IFT-B-connecting tetramer is crucial for ciliogenesis. *J. Cell Biol.* 217, 2867–2876. <https://doi.org/10.1083/jcb.201801039>.
11. Chaya, T., Omori, Y., Kuwahara, R., and Furukawa, T. (2014). ICK is essential for cell type-specific ciliogenesis and the regulation of ciliary transport. *EMBO J.* 33, 1227–1242. <https://doi.org/10.1002/embj.201488175>.
12. Engelke, M.F., Waas, B., Kearns, S.E., Suber, A., Boss, A., Allen, B.L., and Verhey, K.J. (2019). Acute Inhibition of Heterotrimeric Kinesin-2 Function Reveals Mechanisms of Intraflagellar Transport in Mammalian Cilia. *Curr. Biol.* 29, 1137–1148.e4. <https://doi.org/10.1016/j.cub.2019.02.043>.
13. Amanchy, R., Periaswamy, B., Mathivanan, S., Reddy, R., Tattikota, S.G., and Pandey, A. (2007). A curated compendium of phosphorylation motifs. *Nat. Biotechnol.* 25, 285–286. <https://doi.org/10.1038/nbt0307-285>.
14. Blom, N., Gammeltoft, S., and Brunak, S. (1999). Sequence and structure-based prediction of eukaryotic protein phosphorylation sites. *J. Mol. Biol.* 294, 1351–1362. <https://doi.org/10.1006/jmbi.1999.3310>.
15. Blom, N., Sicheritz-Pontén, T., Gupta, R., Gammeltoft, S., and Brunak, S. (2004). Prediction of post-translational glycosylation and phosphorylation of proteins from the amino acid sequence. *Proteomics* 4, 1633–1649. <https://doi.org/10.1002/pmic.200300771>.
16. Hammond, J.W., Blasius, T.L., Soppina, V., Cai, D., and Verhey, K.J. (2010). Autoinhibition of the kinesin-2 motor KIF17 via dual intramolecular mechanisms. *J. Cell Biol.* 189, 1013–1025. <https://doi.org/10.1083/jcb.201001057>.
17. Ichinose, S., Ogawa, T., and Hirokawa, N. (2015). Mechanism of Activity-Dependent Cargo Loading via the Phosphorylation of KIF3A by PKA and CaMKIIa. *Neuron* 87, 1022–1035. <https://doi.org/10.1016/j.neuron.2015.08.008>.
18. Kozeleková, A., Náplavová, A., Brom, T., Gašparik, N., Šimek, J., Houser, J., and Hritz, J. (2022). Phosphorylated and Phosphomimicking Variants May Differ—A Case Study of 14-3-3 Protein. *Front. Chem.* 10, 835733. <https://doi.org/10.3389/fchem.2022.835733>.
19. Plotnikova, O.V., Pugacheva, E.N., and Golemis, E.A. (2009). Primary cilia and the cell cycle. *Methods Cell Biol.* 94, 137–160. [https://doi.org/10.1016/s0091-679x\(08\)94007-3](https://doi.org/10.1016/s0091-679x(08)94007-3).
20. Hopkins, A.L., and Groom, C.R. (2002). The druggable genome. *Nat. Rev. Drug Discov.* 1, 727–730. <https://doi.org/10.1038/nrd892>.
21. Kim, Y.J., and Kim, J. (2019). Therapeutic perspectives for structural and functional abnormalities of cilia. *Cell. Mol. Life Sci.* 76, 3695–3709. <https://doi.org/10.1007/s00018-019-03158-6>.
22. Stokman, M.F., Saunier, S., and Benmerah, A. (2021). Renal Ciliopathies: Sorting Out Therapeutic Approaches for Nephronophthisis. *Front. Cell Dev. Biol.* 9, 653138. <https://doi.org/10.3389/fcell.2021.653138>.
23. Engelke, M.F., Winding, M., Yue, Y., Shastry, S., Teloni, F., Reddy, S., Blasius, T.L., Soppina, P., Hancock, W.O., Gelfand, V.I., et al. (2016). Engineered kinesin motor proteins amenable to small-molecule inhibition. *Nat. Commun.* 7, 11159. <https://doi.org/10.1038/ncomms11159>.
24. Good, J.A., Skoufias, D.A., and Kozielski, F. (2011). Elucidating the functionality of kinesins: an overview of small molecule inhibitors. *Semin. Cell Dev. Biol.* 22, 935–945. <https://doi.org/10.1016/j.semcdb.2011.09.023>.
25. Gailey, C.D., Wang, E.J., Jin, L., Ahmadi, S., Brautigan, D.L., Li, X., Xu, W., Scott, M.M., and Fu, Z. (2021). Phosphosite T674A mutation in kinesin family member 3A fails to reproduce tissue and ciliary defects characteristic of CLK1 loss of function. *Dev. Dynam.* 250, 263–273. <https://doi.org/10.1002/dvdy.252>.
26. Oh, Y.S., Wang, E.J., Gailey, C.D., Brautigan, D.L., Allen, B.L., and Fu, Z. (2019). Ciliopathy-Associated Protein Kinase ICK Requires Its Non-Catalytic Carboxyl-Terminal Domain for Regulation of Ciliogenesis. *Cells* 8, 677. <https://doi.org/10.3390/cells8070677>.
27. Wang, E.J., Gailey, C.D., Brautigan, D.L., and Fu, Z. (2020). Functional Alterations in Ciliogenesis-Associated Kinase 1 (CLK1) that Result from Mutations Linked to Juvenile Myoclonic Epilepsy. *Cells* 9, 694. <https://doi.org/10.3390/cells9030694>.
28. Pirkmajer, S., and Chibalin, A.V. (2011). Serum starvation: caveat emptor. *Am. J. Physiol. Cell Physiol.* 301, C272–C279. <https://doi.org/10.1152/ajpcell.00091.2011>.
29. Rashid, M., and Coombs, K.M. (2019). Serum-reduced media impacts on cell viability and protein expression in human lung epithelial cells. *J. Cell. Physiol.* 234, 7718–7724. <https://doi.org/10.1002/jcp.27890>.
30. Seeger, M.A., Zhang, Y., and Rice, S.E. (2012). Kinesin tail domains are intrinsically disordered. *Proteins: Struct., Funct., Bioinf.* 80, 2437–2446. <https://doi.org/10.1002/prot.24128>.
31. Michel Espinoza-Fonseca, L. (2012). Aromatic residues link binding and function of intrinsically disordered proteins. *Mol. Biosyst.* 8, 237–246. <https://doi.org/10.1039/c1mb05239j>.
32. Prevo, B., Scholey, J.M., and Peterman, E.J.G. (2017). Intraflagellar transport: mechanisms of motor action, cooperation, and cargo delivery. *FEBS J.* 284, 2905–2931. <https://doi.org/10.1111/febs.14068>.
33. Tang, C., Wu, X., Ren, Q., Yao, M., Xu, S., and Yan, Z. (2022). Hedgehog signaling is controlled by Rac1 activity. *Theranostics* 12, 1303–1320. <https://doi.org/10.7150/thno.67702>.
34. Phang, H.-Q., Hoon, J.-L., Lai, S.-K., Zeng, Y., Chiam, K.-H., Li, H.-Y., and Koh, C.-G. (2014). POPX2 phosphatase regulates the KIF3 kinesin motor complex. *J. Cell Sci.* 127, 727–739. <https://doi.org/10.1242/jcs.126482>.
35. Ludington, W.B., Wemmer, K.A., Lechtreck, K.F., Witman, G.B., and Marshall, W.F. (2013). Avalanched-like behavior in ciliary import. *Proc. Natl. Acad. Sci. USA* 110, 3925–3930. <https://doi.org/10.1073/pnas.1217354110>.

36. Wemmer, K., Ludington, W., and Marshall, W.F. (2020). Testing the role of intraflagellar transport in flagellar length control using length-altering mutants of *Chlamydomonas*. *Phil. Trans. R. Soc. B* 375, 20190159. <https://doi.org/10.1098/rstb.2019.0159>.
37. Verhey, K.J., and Hammond, J.W. (2009). Traffic control: regulation of kinesin motors. *Nat. Rev. Mol. Cell Biol.* 10, 765–777. <https://doi.org/10.1038/nrm2782>.
38. Nievergelt, A.P., Zykov, I., Diener, D., Chhatre, A., Buchholz, T.-O., Delling, M., Diez, S., Jug, F., Štěpánek, L., and Pigino, G. (2022). Conversion of anterograde into retrograde trains is an intrinsic property of intraflagellar transport. *Curr. Biol.* 32, 4071–4078.e4. <https://doi.org/10.1016/j.cub.2022.07.033>.
39. Schindelin, J., Arganda-Carreras, I., Frise, E., Kaynig, V., Longair, M., Pietzsch, T., Preibisch, S., Rueden, C., Saalfeld, S., Schmid, B., et al. (2012). Fiji: an open-source platform for biological-image analysis. *Nat. Methods* 9, 676–682. <https://doi.org/10.1038/nmeth.2019>.
40. Hartley, M., Kleywegt, G.J., Patwardhan, A., Sarkans, U., Swedlow, J.R., and Brazma, A. (2022). The BioImage Archive – Building a Home for Life-Sciences Microscopy Data. *J. Mol. Biol.* 434, 167505. <https://doi.org/10.1016/j.jmb.2022.167505>.
41. Norris, S.R., Nunez, M.F., and Verhey, K.J. (2015). Influence of fluorescent tag on the motility properties of kinesin-1 in single-molecule assays. *Biophys. J.* 108, 1133–1143. <https://doi.org/10.1016/j.bpj.2015.01.031>.
42. Shaner, N.C., Lambert, G.G., Chammas, A., Ni, Y., Cranfill, P.J., Baird, M.A., Sell, B.R., Allen, J.R., Day, R.N., Israelsson, M., et al. (2013). A bright monomeric green fluorescent protein derived from *Branchiostoma lanceolatum*. *Nat. Methods* 10, 407–409. <https://doi.org/10.1038/nmeth.2413>.
43. Ho, S.N., Hunt, H.D., Horton, R.M., Pullen, J.K., and Pease, L.R. (1989). Site-directed mutagenesis by overlap extension using the polymerase chain reaction. *Gene* 77, 51–59. [https://doi.org/10.1016/0378-1119\(89\)90358-2](https://doi.org/10.1016/0378-1119(89)90358-2).
44. Horton, R.M., Hunt, H.D., Ho, S.N., Pullen, J.K., and Pease, L.R. (1989). Engineering hybrid genes without the use of restriction enzymes: gene splicing by overlap extension. *Gene* 77, 61–68. [https://doi.org/10.1016/0378-1119\(89\)90359-4](https://doi.org/10.1016/0378-1119(89)90359-4).

STAR★METHODS

KEY RESOURCES TABLE

REAGENT or RESOURCE	SOURCE	IDENTIFIER
<b>Antibodies</b>		
Rabbit anti-ARL13B	Protein Tech Group	Cat# 17711-1-AP; RRID: AB_2060867; Lot 00103765
Mouse anti-myc	Millipore Sigma	Cat# M4439; RRID: AB_439694; Clone 9e10; Lot 029M4849V
<b>Chemicals, peptides, and recombinant proteins</b>		
Lipofectamine 2000	ThermoFisher Scientific	Cat# 11668019
<b>Deposited data</b>		
Non-destructively annotated epifluorescence microscopy images	This study	BioImage Archive: <a href="https://www.ebi.ac.uk/biostudies/bioimages/studies/S-BIAD748?key=44348562-d945-4568-aaad-55738fdc8854">https://www.ebi.ac.uk/biostudies/bioimages/studies/S-BIAD748?key=44348562-d945-4568-aaad-55738fdc8854</a>
<b>Experimental models: Cell lines</b>		
Kif3a <sup>-/-</sup> ; Kif3b <sup>-/-</sup> 3T3 cells	Engelke et al., 2019 <sup>12</sup>	N/A
<b>Oligonucleotides</b>		
Primers to amplify and clone the KIF3B tail 5'-gtccgagatggccgatct-3' 5'-gcgatggatcctcacctagtattgcagcaggctatcgatca-3'	This study	N/A
Annealed primers yield Flag-tag Insertable via restriction sites AgeI and BstEII 5'-ccggttgactacaaagacgatgacgacaagtag-3' 5'-gtcacctactgtgctcatcgtctttgtagtaa-3'	This study	N/A
Primers for generating single point mutations in KIF3A tail, see Table S1	This study	N/A
<b>Recombinant DNA</b>		
pmNeonGreen-N1 (mNG)	Engelke et al., 2019 <sup>12</sup>	N/A
pmCherry-N1 (mCherry)	Engelke et al., 2019 <sup>12</sup>	N/A
MmKIF3B-mNeonGreen	This study	N/A
MmKIF3B-mCherry	Engelke et al., 2019 <sup>12</sup>	N/A
HA-MmKIF3B	This study	N/A
HA-mCherry-MmKIF3B	This study	N/A
MmKIF3A	Engelke et al., 2019 <sup>12</sup>	N/A
myc-MmKIF3A	This study	N/A
MmKIF3A(S698A)	This study	N/A
MmKIF3A(T694A)	This study	N/A
MmKIF3A(S689A)	This study	N/A
MmKIF3A(S675A)	This study	N/A
MmKIF3A(T674A)	This study	N/A
MmKIF3A(S665A)	This study	N/A
MmKIF3A(S661A)	This study	N/A
MmKIF3A(T658A)	This study	N/A
MmKIF3A(S698D)	This study	N/A
MmKIF3A(T694D)	This study	N/A
MmKIF3A(S689D)	This study	N/A

(Continued on next page)

**Continued**

REAGENT or RESOURCE	SOURCE	IDENTIFIER
MmKIF3A(S675D)	This study	N/A
MmKIF3A(T674D)	This study	N/A
MmKIF3A(S665D)	This study	N/A
MmKIF3A(S661D)	This study	N/A
MmKIF3A(T658D)	This study	N/A
myc-MmKIF3A(5xD/E)	This study	N/A
myc-MmKIF3A(8xA)	This study	N/A
3xFlag-MmKIF3A(8xA)	This study	N/A
MmKIF3A(8xA)-Flag	This study	N/A
myc-MmKIF3A(8xD)	This study	N/A
myc-MmKIF3A(11xA/F)	This study	N/A
myc-MmKIF3A(11xD/E)	This study	N/A
myc-MmKIF3A(16xA/F)	This study	N/A
myc-MmKIF3A(16xD/E)	This study	N/A
myc-MmKIF3A(Y609E)	This study	N/A
myc-MmKIF3A(T627D)	This study	N/A
myc-MmKIF3A(S651D)	This study	N/A
myc-MmKIF3A(Y654E)	This study	N/A
myc-MmKIF3A(Y657E)	This study	N/A
myc-MmKIF3A(T627D/Y657E)	This study	N/A
myc-MmKIF3A(T627N/Y657Q)	This study	N/A
myc-MmKIF3A(T627A/Y657F)	This study	N/A
myc-MmKIF3A(T627D/S698D)	This study	N/A
myc-MmKIF3A(Y657E/S698D)	This study	N/A
myc-MmKIF3A(T627D/Y657E/S698D)	This study	N/A

**Software and algorithms**

Image J with FIJI 2.1.1	Schindelin et al., <sup>39</sup>	<a href="https://imagej.net/software/fiji/">https://imagej.net/software/fiji/</a> RRID: SCR_002285
GraphPad Prism 9.4.1	GraphPad Software	<a href="https://www.graphpad.com/">https://www.graphpad.com/</a> RRID:SCR_002798
Adobe Illustrator 27.6	Adobe	<a href="https://www.adobe.com/products/illustrator.html">https://www.adobe.com/products/illustrator.html</a> RRID:SCR_010279
NetPhos3.1	Blom et al., <sup>14</sup> Blom et al., <sup>15</sup>	<a href="https://services.healthtech.dtu.dk/services/NetPhos-3.1/">https://services.healthtech.dtu.dk/services/NetPhos-3.1/</a> RRID:SCR_017975
PhosphoMotif Finder	Amanchy et al., <sup>13</sup>	<a href="http://www.hprd.org/PhosphoMotif_finder">http://www.hprd.org/PhosphoMotif_finder</a>

**RESOURCE AVAILABILITY**

**Lead contact**

Further information and requests for resources and reagents should be directed to and will be fulfilled by the lead contact, Martin F. Engelke ([mfengel@ilstu.edu](mailto:mfengel@ilstu.edu)).

**Materials availability**

Plasmids generated in this study will be provided upon request from the **lead contact**, Martin F. Engelke ([mfengel@ilstu.edu](mailto:mfengel@ilstu.edu)).

**Data and code availability**

- All original image data have been deposited in the Biolineage Archive<sup>40</sup> (<https://www.ebi.ac.uk/bioimage-archive/>). They will be publicly available via accession number S-BIAD748 as of the publication date.
- This paper does not report original code.
- Any additional information required to reanalyze the data reported in this paper is available from the **lead contact** upon request.

## EXPERIMENTAL MODEL AND STUDY PARTICIPANT DETAILS

*Kif3a*<sup>-/-</sup>; *Kif3b*<sup>-/-</sup> double knockout 3T3 cells were generated and are described in.<sup>12</sup> They were generated via CRISPR/Cas9-mediated knockout from the parental cell line NIH 3T3 Flp-In (*Mus musculus* embryonic fibroblast; RRID: CVCL\_U422) purchased from Thermo Fisher Scientific. The *Kif3a*<sup>-/-</sup>; *Kif3b*<sup>-/-</sup> 3T3 cells were cultured in DMEM (Corning) supplemented with 10% Fetal Clone III (Cytiva Hyclone) and 4 mM L-glutamine (Alfa Aesar) at 37°C and 5% CO<sub>2</sub>. Subculturing was performed to keep cells between 4 to 80% confluent. The cells have a male karyotype, but since we are studying fundamental processes in motor function and ciliogenesis and these mechanisms are found in all cells, we have no reason to expect differences based on sex. The presence of the double knockout is regularly re-authenticated via the rescue of ciliogenesis by co-transfection with plasmids driving the expression of KIF3A and KIF3B. All cells in the lab are periodically tested for mycoplasma contamination via a commercially available PCR test (ATCC).

## METHOD DETAILS

### Bioinformatic analysis

NetPhos3.1<sup>14,15</sup> and PhosphoMotif Finder<sup>13</sup> were used to identify potential phosphorylation sites in the KIF3A tail domain.

### Expression plasmids

Below, protein sequences are shown in capitalized letters in standard single-letter code, and DNA sequences are shown in lowercase letters. The names of all used or generated constructs are shown in bold letters. All DNA synthesis was performed by Twist Bioscience.

Plasmids encoding mCherry (mChe), MmKIF3A, MmKIF3B, MmKIF3A-mNG, and MmKIF3B-mChe were described previously.<sup>12,41</sup> pmNeonGr-N1 (soluble mNG) was generated by PCR amplifying the mNeonGreen<sup>42</sup> (Allele Biotechnologies) open reading frame (ORF) from MmKIF3A-mNG, using the primers 5'-ttatatACCGGTCCGCCACCATGGTGAGCAAGGGCG-3' and 5'-TFACTTGACAGCTCGTCC ATGC-3' to add an AgeI and Kozak consensus sequence on the 5' end and inserting it into pmCherry-N1 (Clontech Cat# 632523) via AgeI and BsrGI. To clone a plasmid encoding myc-MmKIF3A, a DNA fragment encoding the Myc-tag (M-EQKLISEEDL), followed by the linker GYYK and the N-terminal sequence of *Mm* KIF3A, was synthesized and cloned into the plasmid encoding *Mm* KIF3A using the restriction enzymes NheI and KpnI. To generate plasmid KIF3B-mNG, the ORF for mNG was excised from MmKIF3A-mNG and cloned in place of mChe into plasmid MmKIF3B-mChe using the restriction enzymes BamHI and BsrGI. Plasmids encoding HA-MmKIF3B and HA-mChe-MmKIF3B were cloned by synthesizing ORFs encoding the HA-tag (M-YPYDVPDYA) followed by the linker GGRP via restriction sites NheI and SacI and the N-terminal sequence of MmKIF3B or encoding an HA-tag fused via the linker GSGSGRP to mChe which in turns fused via the linker RTGSGSGSGT to the N-terminal sequence of MmKIF3B via restriction sites NheI and Sall into the vector encoding *Mm* KIF3B.

Following bioinformatic analysis, we used Splice by Overlap Extension (SOE) PCR<sup>43,44</sup> and Gibson Assembly (NEBuilder, NEB) to mutate single identified potential phosphorylation sites to (A) or (F) to mimic the dephosphorylated state or (D) or (E) to mimic the phosphorylated state in the KIF3A tail domain. The amplified tail domain was subsequently subcloned via the restriction sites BamHI and PstI into the MmKIF3A plasmid to generate the plasmids T658A, T658D, S661A, S661D, S665A, S665D, T674A, T674D, S675A, S675D, S689A, S689D, T694A, T694D, S698A, and S698D. The primer sequences and methods used to create these phosphomimetic mutant plasmids are shown in Table S1. Additional plasmids encoding MmKIF3A with single selected amino acids (T627D, S651D, Y654E, Y657E, Y699E) and multiple selected amino acids (T627D-Y657E, T627N-Y657Q, T627D-Y657E-S698D) in the tail domain mutated were cloned by synthesizing DNA fragments encoding the mutated tail domain and subcloning them via the restriction sites PstI and BamHI into the plasmid encoding myc-MmKIF3A. To generate the plasmids encoding T627D-S689D and Y657E-S698D, T627D and Y657E were used as backbones. The mutation S698D was introduced via a site-directed mutagenesis PCR (QuikChange II XL kit, Agilent) using the primers 5'-agtgatcgtgatcctgctg caataactaggtgag-3' and 5'-gcagcaggtcatcgtactgtctctggctt-3'. Plasmids encoding MmKIF3A with five (5xD/E), eight (8xA, 8xD), eleven (11xA/F, 11xD/E), or sixteen (16xA/F, 16xD/E) potential mutated phosphorylation sites were cloned by synthesizing DNA fragment encoding the mutant KIF3A tail domain and subcloning into the vector encoding myc-MmKIF3A via the restriction sites PstI and BamHI. A plasmid encoding an N-terminal Flag-tagged MmKIF3A(8xA) was generated by annealing the oligos 5'-ccggttgactacaagacgatgacgacaagtag-3' and 5'-gtcacctactgtgctgcatcgtctttagtagca-3' and subcloning this Flag-tag ORF (DYKDDDDK) via restriction sites AgeI and BstEII into plasmid MmKIF3A(8xA). A plasmid encoding C-terminally 3xFlag-tagged MmKIF3A(8xA) was created by synthesizing a 3xFlag tag (M-DYKDHDG-DYKDHDIDYKDDDDK) followed by the linker GARAG and the N-terminal sequence of KIF3A and cloning it via restriction sites NheI and KpnI into MmKIF3A(8xA).

### Cell culture techniques, immunofluorescence, and microscopy

*Kif3a*<sup>-/-</sup>; *Kif3b*<sup>-/-</sup> double knockout 3T3 cells<sup>12</sup> were cultured in DMEM (Corning) supplemented with 10% Fetal Clone III (Cytiva Hyclone) and 4 mM L-glutamine (Alfa Aesar) at 37°C and 5% CO<sub>2</sub>. For experiments, 1x10<sup>5</sup> cells were seeded on glass coverslips in 12-well plates. Around 16 hours later, cells were transfected using Lipofectamine 2000 (Life Technologies) according to the manufacturer's protocol in DMEM with reduced serum content (1% FetalClone III). Serum starvation stimulates ciliation. Forty-eight hours post-transfection and serum starvation, cells were fixed with 10% buffered formalin (Fisher HealthCare), and immunostaining was performed as previously described.<sup>12</sup> In brief, cells were incubated in 50 mM ammonium chloride in PBS for 10 minutes after formalin fixation to remove unreacted formaldehyde and then permeabilized with 0.2% Triton X-100 in PBS for 5 minutes. Subsequently, cells were incubated in blocking solution (0.2% fish skin gelatin in PBS) for 5 minutes. The following antibodies were diluted into blocking solution and applied: rabbit anti-ARL13B 1:1000 (Proteintech Cat#17711-1-AP;

RRID:AB\_2060867), mouse anti-myc 1:1000 (Sigma-Aldrich Cat# M4439, RRID:AB\_439694), goat anti-mouse-Alexa Fluor 488 1:500 (Molecular Probes Cat# A-11029, RRID:AB\_2534088) and goat anti-rabbit-Alexa Fluor 647 1:500 (Molecular Probes Cat# A-21244; RRID:AB\_2535812). Nuclei were stained with 10.9  $\mu\text{M}$  4',6-diamidino-2-phenylindole (DAPI, Biotium), and coverslips were mounted in ProlongGold (Life Technologies).

### Microscopy and image analysis

Micrographs were acquired using an inverted, semi-automated BZ-X810 epifluorescence microscope (Keyence) using a Plan APOchromate 40x, 0.95 numerical aperture (NA) objective. Images were analyzed with ImageJ software using the FIJI package.<sup>39</sup> Only cells expressing the exogenous motor protein (KIF3A/KIF3B) from low to medium levels were selected for quantification, as done previously.<sup>12</sup> Transfected cells were located in the red (KIF3B) channel, if present, or in the green (KIF3A) channel and the presence of a cilium was evaluated in the ARL13B channel. Cilium length was manually measured (non-destructively annotated in the dataset published with this study), and only cilia longer than 0.5  $\mu\text{M}$  were counted as cilia.

### QUANTIFICATION AND STATISTICAL ANALYSIS

Cells expressing high levels of exogenous kinesin motor proteins were excluded from analysis similarly as in our previous study.<sup>12</sup> For each condition,  $n \geq 43$  (transfected cells) were imaged, and the experiment was repeated three times for a total of  $n \geq 149$  cells per condition, as indicated in the figure legends. Data were graphed using Prism (GraphPad) and are displayed as mean  $\pm$  SD. Prism was also used to perform one-way ANOVA analysis to compare the ciliation rate and cilia length between constructs in each experiment, and the results can be found in the figure legends. Following a significant F-value, Dunnett's post hoc comparison tests were used to identify groups that were significantly different ( $p < 0.05$ ) from cells expressing wildtype KIF3A. No randomization, stratification, blinding, or sample size estimations were performed in this study.